**Annales
Geophysicae**

Fresnel scatter revisited – comparison of 50 MHz radar and radiosondes in the Arctic, the Tropics and Antarctica

S. Kirkwood[1]**, E. Belova**[1]**, K. Satheesan**[1]**, T. Narayana Rao**[2]**, T. Rajendra Prasad**[2]**, and S. Satheesh Kumar**[2]

[1]Swedish Institute of Space Physics, Box 812, 98128 Kiruna, Sweden
[2]National Atmospheric Research Laboratory, Gadanki, India

Abstract. High-resolution radiosondes and calibrated radars operating close to 50 MHz, are used to examine the relationship between the strength of radar scatter and refractive index gradient. Three radars are used, in Kiruna in Arctic Sweden, at Gadanki in southern India and at the Swedish/Finnish base Wasa/Aboa in Queen Maud Land, Antarctica. Calibration is accomplished using the daily variation of galactic noise measured at each site. Proportionality between radar scatter strength and the square of the mean gradient of potential refractive index, M^2, is found in the upper troposphere and lower stratosphere at all three sites, confirming previously reported results from many VHF radars. If the radar scatter is interpreted as Fresnel scatter, the constant of proportionality between radar scatter and M^2 is found to be the same, within the calibration uncertainties, for all three radars. The radiosondes show evidence of distinct layering with sharp gradients, extending over 10s of kilometers horizontally, but the scatter is found to be two orders of magnitude weaker than would be expected from true Fresnel scatter from such layers. Using radar reflectivities resolved to a few 100 ms, we show that this is due to strong temporal variability in the scattering conditions, possibly due to undulations of the scattering layers. The constancy of the radar scatter – M^2 relationship between the different sites suggests an unexpected uniformity in these perturbations between very different regions of the globe.

Keywords. Atmospheric composition and structure (Pressure, density, and temperature) – Meteorology and atmospheric dynamics (Instruments and techniques) – Radio science (Instruments and techniques)

1 Introduction

It has long been apparent that, for radars operating close to 50 MHz, the strength of radar reflection from the troposphere and lower stratosphere is closely related to the static stability of the atmosphere. Most observational studies of this effect have concentrated on the upper troposphere and lower stratosphere, where radar scatter is highly aspect sensitive, i.e. it is much stronger for vertically directed radar beams than when the beam is a few degrees off vertical. A relationship between strong radar scatter and a strong vertical gradient of potential temperature was first noted by Gage and Green (1978) using a 40 MHz radar in Colorado, USA. Gage and co-workers went on to develop a theory of "Fresnel scatter" which explained the radar echoes in terms of partial reflection from a series of sharp gradients in refractive index, extended horizontally to cover several times the Fresnel radius within the radar beam. This theory was able to account for both a dependence of echo strength on static stability (the mean vertical gradient of refractive index, M, is related to static stability), for strong aspect sensitivity, and for an observed proportionality to the length of the radar pulse used to measure the scatter strength (Gage and Green, 1978; Gage et al., 1981, 1985). Doviak and Zrnic (1984), however, showed that it was not necessary for the reflecting structures to be as extensive as supposed in Gage and co-worker's theory, only that the correlation length of the irregularities should be comparable to the radius of the first Fresnel zone. Doviak and Zrnic's work further showed that the Fresnel scatter theory represented one extreme of a more general theory for scatter from refractive index irregularities, the opposite extreme being scatter from isotropic irregularities (with correlation length much less than the Fresnel radius) resulting from turbulence.

Gage et al. (1985) demonstrated proportionality between radar scatter and climatological profiles of M^2 using three

different radars, in Alaska, Peru and Germany. They assumed that the constant of proportionality should vary exponentially with height and were able to obtain a good fit for heights from 8–50 km. However, they were able to calculate absolute values of radar reflectivity, and find a numerical result for the constant of proportionality, for only one radar, Poker Flat. They did not attempt to interpret this numerical value in terms of the theory.

Subsequently, several authors have reported proportionality between radar back scatter and M^2. Tsuda et al. (1988) used measurements from the MU radar in Japan to show that radar scatter was proportional to M^2, in the upper troposphere and lower stratosphere where M^2 is determined by the static stability and radar scatter is aspect sensitive. Tsuda et al. (1988) found that radar scatter was also proportional to M^2 in the lower tropsphere, where M^2 is determined primarily by humidity gradients, and radar scatter is largely isotropic. Hooper et al. (2004) found the same result using the ESRAD radar in Arctic Sweden and showed how this proportionality could be used to retrieve profiles of static stability using radar measurements (conveniently expressed as Ω_B^2, the square of the buoyancy frequency). Luce et al. (2007) using the MU radar in Japan, showed that the proportionality between M^2 and radar scatter holds down to a vertical resolution of 50 m (previous studies have employed between 150 m and 2500 m resolutions). None of these more recent studies have found it necessary to allow for a height dependence in the constant of proportionality however none of them have considered heights above 20 km. None of the recent studies have used calibrated radars to find the absolute value of the constant of proportionality between M^2 and radar scatter. As a result, none of them have discussed this value in quantitative relation to the Fresnel scattering theory.

In this study we use calibrated observations by three radars, and by high-resolution radiosondes, in very different parts of the world (Arctic Sweden, tropical India and Antarctica) to determine quantitatively the relationship between radar scatter and refractive index gradient and to compare with Fresnel scattering theory.

2 Radar scattering models

Two theoretical models of radar scatter are commonly used in interpreting VHF radar scatter from the troposphere and lower stratosphere. The first is the Fresnel scattering model for highly aspect-sensitive radar scatter, as mentioned above. This model is expressed by Gage et al. (1981, 1985), in terms of a normalised power reflection coefficient $|\rho|^2/\Delta r$ which we will refer to as Fresnel scatter:

$$\frac{|\rho|^2}{\Delta r} = F^2(\lambda)M^2 \tag{1}$$

where Δr is the range resolution of the radar measurement, M is usually referred to as the mean vertical gradient of generalised potential refractive index, and is defined in Eq. (3),

and $F(\lambda)$ is a measure of the fine structure of refractive index variations in the vertical direction at half the radar wavelength λ such that $\lambda^2 F^2(\lambda)M^2/4\pi^2$ is the vertical wave number spectrum of generalized potential radio refractive index at wave number $4\pi/\lambda$.

The second model in common use applies to scatter from isotropic irregularities caused by turbulence. In this case scatter is not aspect sensitive and is described by volume reflectivity, η. Assuming that the turbulence is caused by shear instabilities where the shear Richardson number is reduced to a value of 1/4, a quantitative relation between characteristics of the turbulence and the volume reflectivity has been derived by Hocking (1985)

$$\eta = \frac{aL_0^{4/3}M^2}{\lambda^{1/3}} \tag{2}$$

where a is the ratio of eddy diffusion coefficients for potential refractive index and heat, which is close to unity, L_0 is the outer scale length of the turbulence spectrum.

The mean vertical gradient of generalized potential refractive index is given by:

$$M = -77.6 \times 10^{-6} \frac{p}{T} \frac{\delta\ln\theta}{\delta z}\left[1 + \frac{15,500q}{T}\left(1 - \frac{1}{2}\frac{\delta\ln q/\delta z}{\delta\ln\theta/\delta z}\right)\right] \tag{3}$$

where p is pressure in hPa, θ is potential temperature, T temperature, both in K and q is the specific humidity in kg kg^{-1}. In the troposphere and lower stratosphere, M can be determined from radiosondes, and at heights above the mid-troposphere, as we shall see below, only the dry term is important. Note that, when the humidity term is negligible,

$$M = M_D = -77.6 \times 10^{-6} \frac{p}{T} \frac{\delta\ln\theta}{\delta z} = -77.6 \times 10^{-6} \frac{p}{T} \frac{\Omega_B^2}{g} \tag{4}$$

where Ω_B^2 is the bouyancy frequency and g is the acceleration due to gravity.

Each of the models described by Eqs. (1) and (2) represents opposite extremes of a more general theory of radar scatter from refractive index irregularities in the atmosphere as developed, for example, by Doviak and Zrnic (1984). Fresnel scatter applies to the case where the horizontal correlation length of the scatterers is greater that the Fresnel radius, turbulent scatter applies when the horizontal correlation length is comparable to half the wavelength of the probing radar, i.e. comparable to the vertical scale of the irregularities responsible for the scatter. In the real atmosphere, the situation may be somewhere between these two extremes. However, to take a first step to quantitative comparison of theory with observations we will first consider these two extreme cases. If we can measure η or $|\rho^2|$ we can in principle determine F or L_o and determine whether their values are reasonable in terms of the theories.

Measured estimates of Fresnel reflectivity or volume scatter can be calculated from radar observations as follows (Gage et al., 1985; Gage, 1990):

$$\frac{|\rho|^2}{\Delta r} = \frac{P_r}{P_t} \frac{4\lambda^2 r^2}{L_t A_{eff}^2 \Delta r} \tag{5}$$

$$\eta = \frac{P_r}{P_t} \frac{64(2\ln 2)r^2}{\pi L_t V_f A_{eff} \Delta r} \tag{6}$$

where P_t is power delivered to the antenna, P_r is power due to atmospheric scatter received by the antenna, r is the distance to the scattering volume, Δr is the thickness of the volume element along the radar beam, λ is the radar wavelength, A_{eff} is the effective area of the receiving antenna, L_t accounts for losses in the antenna feed on transmission (<1) and V_f expresses the fraction of the scattering volume which is filled with scatterers ($<=1$).

Note that, for the same radar, with the same values of r and Δr

$$\frac{|\rho|^2}{\Delta r} = \frac{4\pi \lambda^2 V_f}{64(2\ln 2)A_{eff}} \eta \tag{7}$$

i.e., the relationship between the two depends primarily on the gain of the antenna ($G = 4\pi A_{eff}/\lambda^2$).

In order to make absolute measurements of η or $|\rho|^2$ we need to know the radar characteristics P_t, A_{eff}, L_t and to be able to measure P_r in physical units (Watts). Generally P_t and L_t are reasonably well characterized by on-site measurements and A_{eff}, by calculations of the antenna gain. All are fairly stable characteristics of the radars.

The power received by the radar can be estimated from the (numerical) output of the receiver/data acquisition system by:

$$P_r = \frac{k_b B \Delta T_{cal}[S_{tot} - (S_{sys} + S_{sky})]}{C_{filt} n_{coh} n_{code} \Delta S_{cal}} \tag{8}$$

where k_b is Boltzman's constant (JK^{-1}), B is the receiver bandwidth (half-power full width in Hz), ΔT_{cal} is the noise temperature of a reference noise source (K), S_{tot} is the total detected power, S_{sys} is the power due to internal system noise, S_{sky} the power due to sky (galactic) noise, ΔS_{cal} is the signal due to the reference noise source, which can be a calibrated electronic noise generator or the range of the (sidereal) daily variation in sky noise, n_{coh} the number of coherent integrations and n_{code} is 1 for an uncoded pulse, otherwise twice the number of bits in the code. C_{filt} is a correction for the attenuation of wide-bandwidth pulses by narrow receiver filters. All of the parameters S are in the same arbitrary units. ($S_{sys} + S_{sky}$) is found by averaging the detected power over range gates where no scattered signal is expected. The daily variation in ($S_{sys} + S_{sky}$) is dominated by the variation in S_{sky}. Note that ($S_{sys} + S_{sky}$) must be evaluated at the same time resolution as the measurements of P_r, while ΔS_{cal} is a single number evaluated as an average of measurements with the noise-injection source in place, or as an average of the
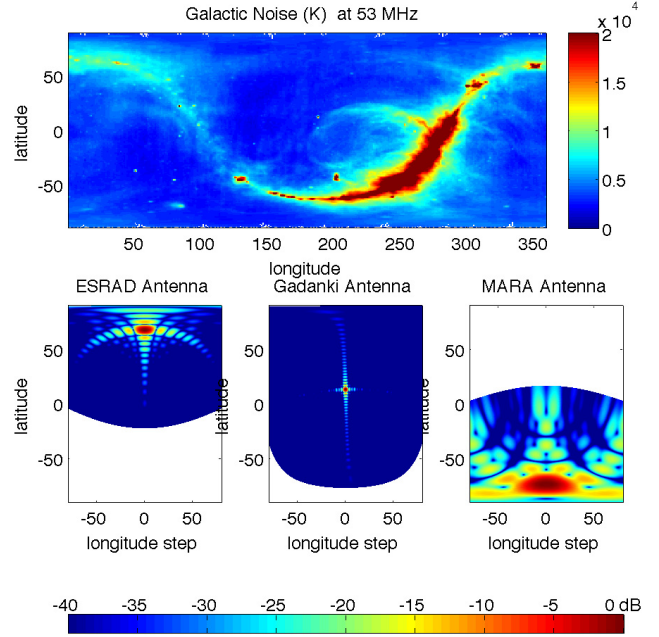

Fig. 1. Upper panel: sky noise at 53 MHz, in celestial equatorial coordinates, from an assimilation of radio-astronomical surveys (de Oliveira-Costa et al., 2008). Lower panels: antenna beam patterns projected to the same coordinate system for the ESRAD, Gadanki and MARA radars.

daily variation of the natural noise over several days. (Calibration using galactic noise is also discussed in Campistron et al., 2001, but the method there is slightly different since it is mainly concerned with passive, rather than active, measurements)

An indication of the degree to which radar scatter may be described by the Fresnel and volume scatter models can be given by the aspect sensitivity, ϕ_s, where the polar diagram of the scatter can be described by the expression

$$I(\phi)/I_0 = \exp\left(\frac{-\sin^2\phi}{\sin^2\phi_s}\right) \tag{9}$$

and ϕ is the angle between the scattering direction and zenith, $I(\phi)$ is the efficiency with which incident radar wave power is scattered at angle ϕ, I_0 is the efficiency at zenith (see e.g. Hocking et al., 1986). Fresnel scattering should lead to very small values of ϕ_s (less than a few degrees), volume scatter to much larger values. In some cases it is possible to estimate ϕ_s from the radar measurements, as will be discussed further in Sect. 4.

3 Radar characteristics and calibration

The main characteristics of the three radars used in this study are summarized in Table 1. Some further description can also be found in Sect. 4 of this paper. It is clear that the radars

Table 1. Main characteristics of the radars used in this study.

Radar	ESRAD	Gadanki MST	MARA-Wasa
Geographic coordinates	68.88° N, 21.10° E	13.46° N, 79.18° E	73.04° S, 13.41° W
Height above sea level	295 m	360 m	470 m
Operating frequency	52 MHz	53 MHz	54.5 MHz
Transmitter peak power	72 kW	2500 kW	20 kW
Antenna effective area	3740 m^2	10 000 m^2	540 m^2
Beam width (1-way, fwhm)	5°	3°	12°
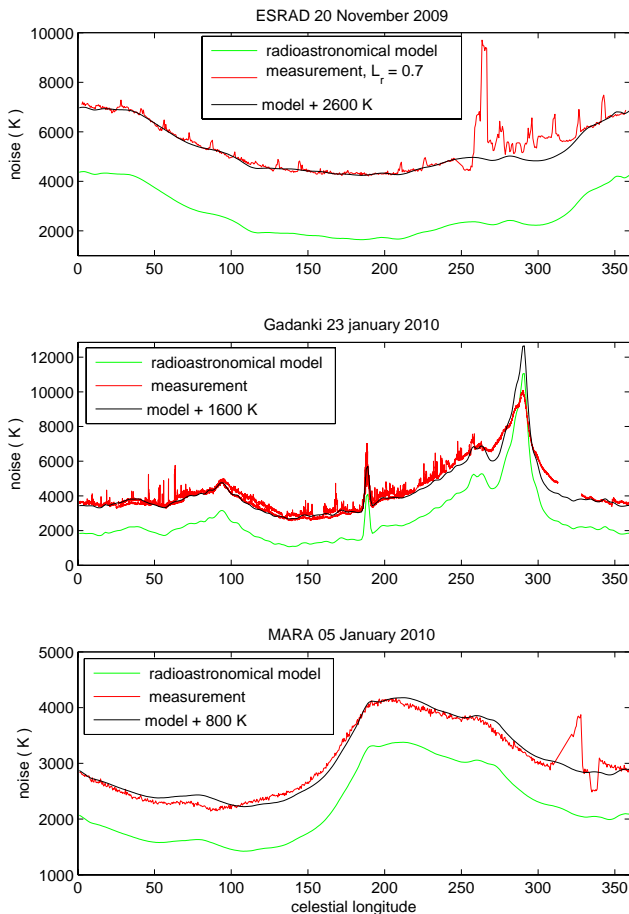
Fig. 2. Comparison of the daily variation of galactic noise for each radar site as predicted by the radio-astronomical empirical model, and measured directly by each radar (for details see text).

are similar in some respects (operating frequency, available height resolution, type of antenna) but differ considerably in others (location, power and antenna effective area). This is further illustrated by the lower panels of Fig. 1 which show the computed antenna beam patterns for each of the three radars. The Gadanki radar has an extremely narrow main beam with highly suppressed sidelobes whereas the ESRAD and particularly MARA radars have broader beams with less

suppressed sidelobes. Note also that the Gadanki antenna array is aligned along geomagnetic coordinates, inclined by 2° (west) to geographic north, whereas the other radar arrays are aligned exaclty along geographic N-S.

In analysing the observations presented later, we will be using the daily variation of galactic noise as the calibration signal for the radars. The upper panel of Fig. 1 shows a sky-map of the galactic noise at 53 MHz. The map has been calculated using software developed and documented by de Oliveira-Costa et al. (2008). This empirical model is based on an assimilation of available radio-astronomical surveys and allows a sky-map to be produced for any frequency. Note, however, that the only data assimilated between 22 MHz and 408 MHz are two surveys at 45 MHz by Maeda et al. (1999) and Alvarez et al. (1997), which have an estimated accuracy of 10% for their temperature scale. In the sky-map, the galactic noise is plotted in celestial coordinates, where the celestial equatorial plane is the projection of the Earth's equatorial plane. The galactic equator, the region where there is the highest density of stars and radio stars, is seen as the band of higher temperatures which winds between northern and southern mid-latitudes. The daily variation of galactic noise as seen by each radar is simply the convolution of the sky-map with the radar beam pattern, with the radar center moving along a line of latitude on the sky map as the the Earth rotates each day. These daily variations are shown by the green curves in the panels in Fig. 2. Note that the noise temperatures seen by the radars are reduced by a factor 2 compared to the sky map since each radar receives only a single polarisation at a time (see e.g. Ellington, 2005).

To confirm that the radars see the same galactic noise variation as they should, according to the radio-astronomical model, each radar has also been calibrated using direct signal (Gadanki) or noise (ESRAD, MARA) injection with artificial sources of known strength. The red lines show the total noise levels measured by the radars on the following (Gadanki) or same (ESRAD, MARA) days as these direct calibrations were made. The black lines show the radio-astronomical model shifted upwards by a constant amount (different for each radar, and determined empirically to give the best fit between the curves) to account for internal noise in the radar systems. It is clear that there is very good agreement, to within 10% everywhere except close to the Galactic
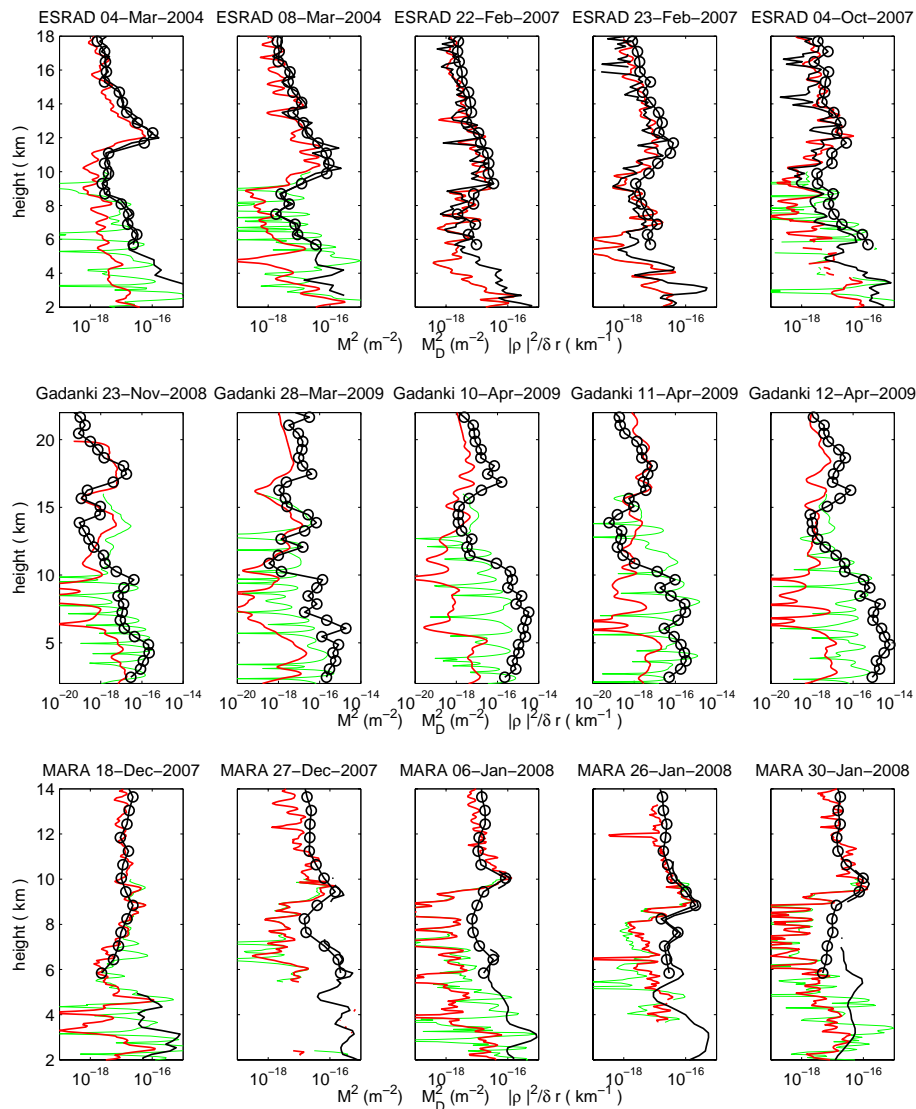
Fig. 3. Comparison of vertical profiles of squared refractive index gradient, M^2 (green) and M_D^2 (red), measured by radiosondes with Fresnel scatter, $|\rho|^2/\Delta r$ measured by the radars (black). Radar measurements marked by small circles were measured with 600 m vertical resolution, those with plain black lines(ESRAD and MARA) were measured with 150 m or 300 m resolution. Note that Fresnel scatter is expressed in units of km^{-1} instead of the usual m^{-1}.

equator crossing at Gadanki. At this time, the noise is so strong that saturation effects limit the radar's ability to measure the signal power correctly. Note that, in Fig. 2, the large discrepancies between the radar measurements and the radio-astronomical model at 250°–300° longitude for ESRAD and at 300°–350° longitude for MARA are caused by artificial noise injection. Further short-lived spikes at ESRAD and Gadanki are due to interference. In conclusion, we can use the amplitude of the variation of the galactic noise as a calibration signal for ESRAD, for MARA and for the Gadanki radar except close to the time of crossing the galactic equator.

Both the ESRAD and MARA radars run continuously over whole 24-h periods so that the whole of the daily variation

can be used for calibration. At Gadanki, experiments are sometimes scheduled for only a few hours so only a small part of the daily variation can be used. This limits the accuracy of the calibration.

4 Comparison of mean reflectivity profiles with M^2

4.1 ESRAD

The ESRAD radar has been in continuous operation since late 1997. More detailed descriptions of the radar and it's usual operating modes can be found in Chilson et al. (1999) and Kirkwood et al. (2007). ESRAD is an interferometric
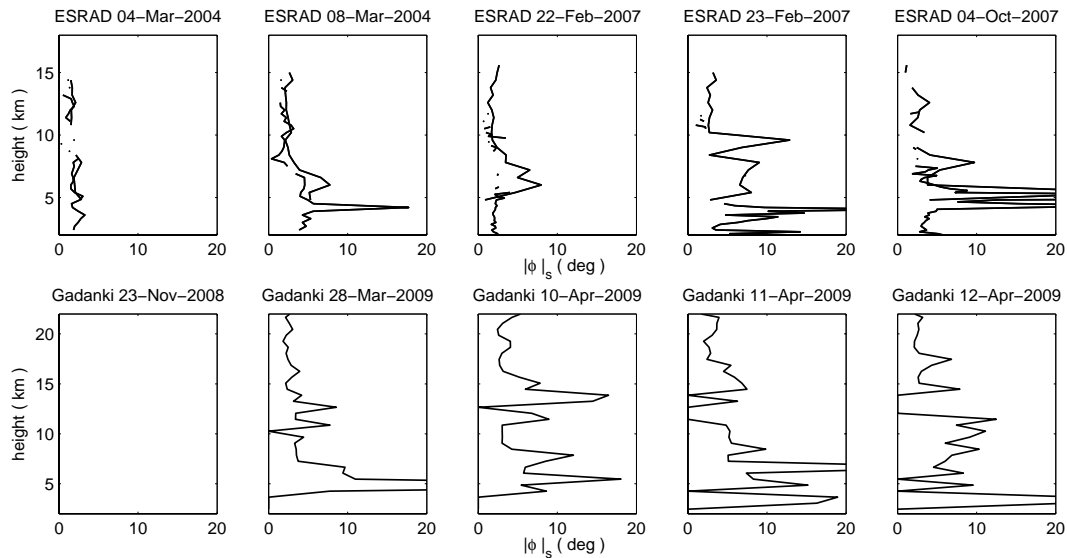
Fig. 4. Aspect sensitivity estimates from ESRAD and the Gadanki radar averaged for the same time intervals as in Fig. 4. See text for further details.

radar with the antenna array divided into 6 sub-arrays, each with its own receiver. For the sonde comparisons, the results from all receivers have been combined in software to correspond to a single vertical radar beam. Several (uncalibrated) comparisons of radar reflectivities with profiles of M or, in the dry upper troposphere-lower stratosphere, with Ω_B^2 for this radar have been published earlier (e.g. Hooper et al., 2004; Kirkwood et al., 2010). The relationship between radar reflectivity and static stability has also been used extensively to identify tropopause folds and intrusions of stratospheric air into the troposphere (e.g. Rao et al., 2008). For our calibrated study here we use measurements from a number of recent occasions when high resolution sondes are available and the characteristics of the radar were reasonably well known, in March 2004, February 2007 and October 2007. For the sondes launched in February 2007, the lower tropospheric winds took the sondes towards the north-west, while those in the upper troposphere carried them towards the south-east, so that they passed very close to the radar site again in the lower stratosphere. These sondes provide a very close comparison with the radar so they are included even though humidity measurements are not available on those occasions. The sondes in March 2004 and February 2007 were standard Vaisala GPS sondes and measurements were recorded with 10 s and 2 s resolution, respectively, during ascent only. We also include measurements from 4 October 2007 when a GPS sonde manufactured by Meteolabor (Switzerland) was used, providing temperature measurements twice per second and recording on both ascent and descent.

For each comparison, the radar measurements of Fresnel scatter and volume reflectivity are averaged for one hour following the sonde launch. Sonde measurements are first averaged to approximately 150 m height resolution using a weighted running mean before calculating M (including the humidity terms) and M_D, the dry term, ignoring humidity terms. These profiles are plotted in the upper panel of Fig. 3, together with profiles of Fresnel scatter from the radar. Radar measurements with both 600 m and 150 m (300 m in March 2004) nominal range resolution are used – these are measured by different operating modes run in alternating time intervals of between 40 s and 160 s. The absolute accuracy of the Fresnel scatter estimates depends on the least well determined parameter in Eq. (5). For the ESRAD radar, which runs continuously, the calibration factor for the estimate of P_r can be determined accurately, to within 10%. The main uncertainty comes from the loss factor L_t which is not monitored continuously and has been found to vary by 30% from an average value of 0.55. So the total absolute accuracy is about 40%. Note that this is the accuracy of the mean value over several days. The relative accuracy for different times and different heights within that period is many times higher.

As can be seen in Fig. 3, the tropopause (where M_D^2 increases sharply) lies between 8–12 km height. The humidity term is sometimes significant below 8 km but, above there, there is close agreement between the shapes of the profiles for M_D^2 and for $|\rho|^2/\Delta r$. At the lower heights, the Fresnel scatter follows roughly the envelope of M^2 but the variability in the latter is high. Note that Fresnel scatter is expressed in units of km^{-1} instead of the usual m^{-1}. This is an arbitary scaling so that the height profiles can be easily compared. The corresponding profiles for η, calculated according to Eq. (6), are not shown. On the logarithmic scale used in Fig. 3 they would simply be parallel to the profiles of $|\rho|^2/\Delta r$, offset by a constant amount according to Eq. (7).
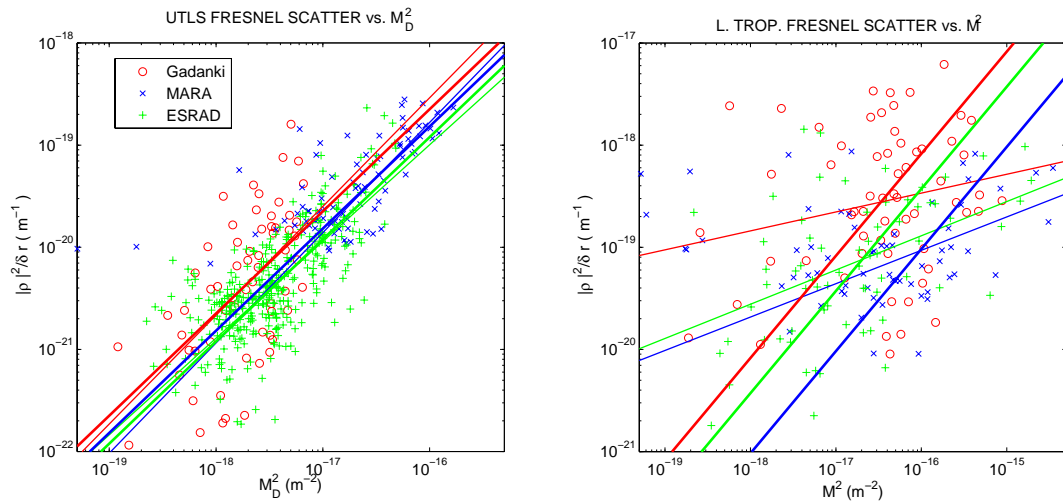
Fig. 5. Scatter plots of squared refractive index gradient, M^2 and M_D^2, measured by radiosondes with Fresnel scatter, $|\rho|^2/\Delta r$ measured by the radars. Left hand plot is for the upper troposphere and lower stratosphere, right hand plot is for the lower troposphere. Two alternative "best fit" lines to all of the points for each radar site are included. For details see text.
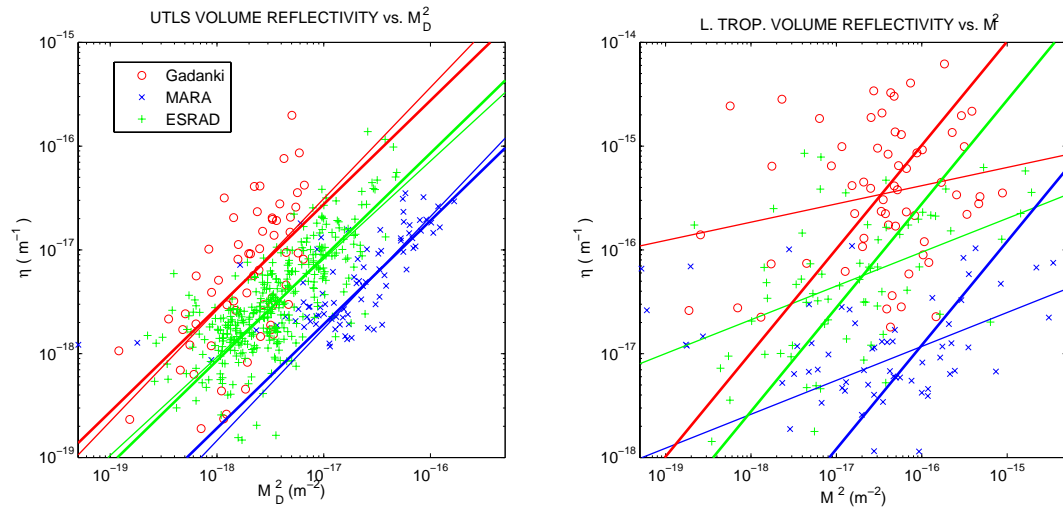

Fig. 6. Scatter plots of squared refractive index gradient, M^2 and M_D^2, measured by radiosondes with volume reflectiviy, η measured by the radars. Left hand plot is for the upper troposphere and lower stratosphere, right hand plot is for the lower troposphere. Two alternative "best fit" lines to all of the points for each radar site are included. For details see text.

An indication of which of the models, volume reflectivity or Fresnel scatter, is likely to be more appropriate, can be found from the aspect sensitivity of the echoes. The top row in Fig. 4 shows profiles of ϕ_s (as defined in Eq. 9) measured using the pattern-scale of the echo structures determined by the full-correlation technique (Holdsworth and Reid, 1995). Profiles of ϕ_s have been averaged over the same time intervals as the profiles in Fig. 3. It is clear that rather low values of ϕ_s are generally seen above 8 km, suggesting Fresnel scatter. The only exception is at about 9 km height on 23 February. Higher values of ϕ_s occur often in the lower troposphere but the values are often not particularly high, and low values

are also seen at some times and heights. This suggests that while more isotropic (volume) scatter occurs in the lower troposphere than above 8 km, Fresnel scatter also occurs in the lower troposphere.

For a statistical comparison with the radar data, the sonde profiles of M^2 and M_D^2 are further averaged with the same range weighting as the radar measurements (150, 300 or 600 m, as appropriate). Scatter plots comparing the values are shown in Figs. 5 and 6. Measurements from 8–18 km height have been used to represent the (dry) upper troposphere and lower stratosphere (UTLS, left hand panels in Figs. 5 and 6). Measurements from 2–5 km height represent

the lower troposphere (right hand panels in Figs. 5 and 6). Least squares fits between logarithms of radar reflectivities and M_D^2 (UTLS) and M^2 (lower troposphere) have been made, and are shown by the straight lines through the points. The different fits are discussed further in Sect. 5. Green symbols and lines represent the ESRAD measurements in Figs. 5 and 6.

4.2 Gadanki MST radar

The Gadanki MST radar has been in operation since 1993 and a technical description can be found in Rao et al. (1995). Previous results comparing radar reflectivities with sondes have been published by Ghosh et al. (2004). The Gadanki MST radar is a Doppler beam-swing radar with a single receiver. Results from experiments using vertical beam only, or with fast switching between vertical beam and one off-vertical beam, have been used. These are a number of special experiments when measurements were made over periods of several hours, and data was recorded with high time resolution, primarily to study mesospheric echoes (Belova et al., 2010). Between 50% and 90% of the transmit/receive arrays were in use in on different occasions, the rest being unavailable due to technical problems. This has been taken into account in calculating reflectivities. The main uncertainty in absolute values of reflectivity for this radar is uncertainty in the calibration factor for P_r due to the short duration of the experiments (2–6 h) and the presence of interfering noise. This restricts the absolute accuracy to about a factor 2, i.e. the true reflectivities may be as little as half and as much as twice the values we calculate.

Radiosondes are launched close to 17:30 LT (12:00 UT) each day. The radar measurements to be used for comparison ended usually at around 16:30 LT, so the radar data has been averaged for the last 30 min of operation. Standard GPS sondes (Meisei RS-01GII) were used, recording at 1 s time intervals, on both ascent and descent. The sonde profiles have been averaged for comparison with radar measurements in the same way as for ESRAD. Note that only radar measurements with 600 m height resolution are available in these comparisons. Only vertical beam measurements have been used for reflectivity calculations to compare with the sonde profiles.

The middle panel of Fig. 3 compares sonde and radar profiles for Gadanki, in the same way as for ESRAD in the top panel. The tropopause height is much higher than at ESRAD, at about 16–17 km, as is expected in the tropics. It is clear that the humidity term is large and significant all the way up to 10–14 km altitude. There is good agreement between the shapes of the profiles for $|\rho|^2/\Delta r$. and M_D^2 above 14 km, and with the envelope of M^2 at lower heights, but the variability in the latter is again high.

Again, we can use measurements of the aspect sensitivity of the echoes to give an indication of which of the models, volume or Fresnel scatter, is likely to be more appropriate.

The second row in Fig. 4 shows profiles of ϕ_s (as defined in Eq. 9) measured using the difference in backscattered power measured for the vertical radar beam and for a beam directed 3° off zenith towards the north. Measurements in the two positions were made in alternate 40 s periods during 4 of the 5 experiments which we use for this study. The method for calculating ϕ_s in this case is as described by (Hocking, 2001). Profiles of ϕ_s are based on averages over the same time intervals as the profiles in Fig. 3. It is again clear that rather low values of ϕ_s are generally seen at the upper heights, above 15 km, suggesting Fresnel scatter, whereas higher values occur at lower heights, particularly in the lower troposphere below 8 km. Again, the high values in the troposphere are often not particularly high, and low values are also seen at some times and heights. So, while more isotropic (volume) scatter occurs in the troposphere than above 15 km, Fresnel scatter also may occur in the troposphere.

Further comparison between radar reflectivities and M^2 and M_D^2 for the Gadanki radar is shown by the red symbols in Figs. 5 and 6, averaged in the same way as for ESRAD. The range chosen to represent the UTLS to 14–22 km. Measurements from 2.6–10 km height are used to represent the lower troposphere

4.3 MARA

The MARA radar has operated only for short periods of a few weeks each, during Antarctic summer seasons, since early 2007. More detailed descriptions of the radar and it's usual operating modes can be found in Kirkwood et al. (2007, 2008). MARA is an interferometric radar with the antenna array divided into 3 sub-arrays, each with its own receiver. Again, the results from all receivers have been combined in software to correspond to a single vertical radar beam. MARA is the best calibrated of the three radars and the absolute accuracy of reflectivities is estimated to be about 20%. We use here measurements from the 2007/2008 season when 5 radiosondes were launched. These were GPS sondes manufactured by Meteolabor, providing temperature mesurements twice per second, recording on both ascent and descent.

Individual profiles comparing sonde and radar measurements can be found in the lowest panel in Fig. 3. Radar measurements with both 600 m and 150 m (300 m in January 2008) nominal range resolution are used – these are measured by different operating modes run in alternating time intervals of between 20 s and 40 s. Sonde measurements and radar data were averaged in the same ways as for ESRAD. The tropopause can be seen at typical polar heights, between 6 km and 10 km. The humidity term in M^2 sometimes becomes significant below 4–5 km. Otherwise there is a close agreement between the shapes of the profiles for M_D^2 and for $|\rho|^2/\Delta r$, except where M^2 is very low in the upper troposphere. This is an artefact of the rather large beam width for MARA – in the absence of any detectable signal from directly overhead, strong echoes from lower altitudes at

off-zenith angles lead to false echo power. To avoid this we restrict the range chosen to represent the UTLS to 8–14 km. Measurements from 2–5 km height are used to represent the lower troposphere. Blue symbols and lines in Figs. 5 and 6 show the observations from MARA, in the same way as described for ESRAD.

In the case of MARA, we are not able to make reliable estimates of the aspect sensitivity of the echoes. This is partly due to the low power-aperture product which leads to weak echoes, and partly to the small size of the antenna array which leads to underestimates of the echo-structure pattern scale when applying the full-correlation analysis technique (Holdsworth, 1999).

5 Relation between M^2, M_D^2 and reflectivity

The relationships between M^2, M_D^2, Fresnel scatter and volume reflectivity for the dry UTLS region and the humid lower troposphere are summarised in Figs. 5 and 6 (representing the same measurements as shown in Fig. 3, i.e. 5 radiosonde/radar profiles at each site). Two straight-line fits are shown for each data set. The thick line assumes that $|\rho|^2/\Delta r$ or η are proportional to M^2 or M_D^2, which is the result found in earlier, more extensive, radiosonde-radar comparisons at ESRAD (Hooper et al., 2004) and at several other radars (see introduction). The fit determines the constant of proportionality, which corresponds to the vertical position of each line in the figures, i.e. different constants of proportionality at different sites lead to vertical offsets between the lines.

The thin lines are best fits to $\log(|\rho|^2/\Delta r)$ or $\log(\eta) = \log(B(M^2)^A)$ or $\log(B(M_D^2)^A))$, where A and B are parameters to be determined by the fitting (i.e. A is not set to unity which is the case in the fits represented by the thick lines). The fit is a standard regression line, i.e. it assumes the values of M^2 or M_D^2 are error-free, and minimises the variance between the line and $\log(|\rho|^2/\Delta r)$ or $\log(\eta)$. This is a reasonable approach if we assume that the radiosondes give a very accurate measure of the state of the refractive index gradient and the radar measurements represent a geophysically variable response, for example through variations in $F^2(\lambda)$ or in L_0 in Eqs. (1) and (2). Here we need to consider further the uncertainty in the radiosonde measurements.

In the UTLS, the accuracy of $M^2 \approx M_D^2$ determined from the radiosonde profiles depends on the accuracy with which the potential temperature gradient can be determined. If we assume that radiosonde temperature measurements have a random uncertainty of 0.2 C, a possible bias up to 0.5 C, with corresponding uncertainties for pressure 1 hPa and 0.5 hPa (e.g. as in the manufacturers specifications), we can estimate the uncertainty of M_D^2 for typical atmospheric conditions using numerical simulation. Allowing for smoothing over 150 m in height (about 30 samples) before calculating potential temperature gradient, we find that the uncertainty in M_D^2 should be better than 1% at the upper end of our ob-

servation range ($M_D^2 = 10^{-16}$) increasing to about 30% at the lower end ($M_D^2 = 10^{-18}$). The uncertainties are primarily due to the random errors rather than possible biases. The random errors and possible biases in radiosonde relative humidity measurements are, at best, of order 2% and 5% respectively. As a result, in the lower troposphere, where the humidity term becomes important, uncertainties in M^2 can become rather large, at least 3 times those in the UTLS. As a consequence, the assumption that radiosondes give an accurate measure of M^2 is more reasonable in the UTLS than in the lower troposphere.

Considering both Fig. 5 and Fig. 6, it is clearly the observations cluster closer to straight lines, and the two fitted lines for each data-set are closer to each other, in the UTLS, with much more spread in the lower troposphere. The spread in all cases is more than we would expect from the accuracy of our radar reflectivity estimates (which is between 20% and a factor 2). Some of the spread could be due to geophysical variations in the fine structure terms $F(\lambda)$ or L_o in Eqs. (1) and (2). It can also be due to spatial and (in the case of Gadanki) temporal differences between the radar measurements and the sonde profiles. Such differences are likely to be most important in the lower troposphere, where the humidity plays a substantial role. In the UTLS, the two fitted lines for each data-set have very close to the same slope, showing that our data-set is consistent with earlier studies. In the lower troposphere there is a substantial discrepancy between the slope of the two fitted lines at each radar. This is consistent with the possibility that radiosonde-based estimates of M^2 are less accurate and that the spatial-temporal variability is stronger at these heights, so that the fitting assumption for the thin line may not be appropriate. We note that the fits assuming direct proportionality (thick lines) give a visually good fit to the observations, in agreement with earlier, more extensive studies. Here we are not primarily concerned with the slopes of the fitted lines but rather their offsets in the vertical direction, which represent the proportionality constant between radar reflectivity and M^2. So we concentrate on the fits represented by the thick lines.

For Fresnel scatter in the UTLS (Fig. 5), all radars have very close to the same constant of proportionality (i.e. the offset of the fitted lines in the vertical direction is small). The fits give $|\rho|^2/\Delta r = 1.0 - 2.0 \times 10^{-3} \times M_D^2$ for ESRAD and MARA and $1 - 7 \times 10^{-3} \times M_D^2$ for Gadanki. (Here we quote 95% confidence limits based taking into account both the statistical confidence of the fits and the estimated absolute uncertainties in calibration given in the previous section, the latter being 40%, a factor 2 and 20% for ESRAD, Gadanki and MARA, respectively.) Close to the same constant of proportionality was found for the Poker Flat radar by Gage et al. (1985), i.e. $|\rho|^2 \Delta r = F^2(\lambda)M^2$, with $F^2(\lambda) = 6 \times 10^{-3}$ at 10 km height (unfortunately with no uncertainty estimate given). This is a remarkable result since it implies that, if the Fresnel scattering model is correct, the average fine structure
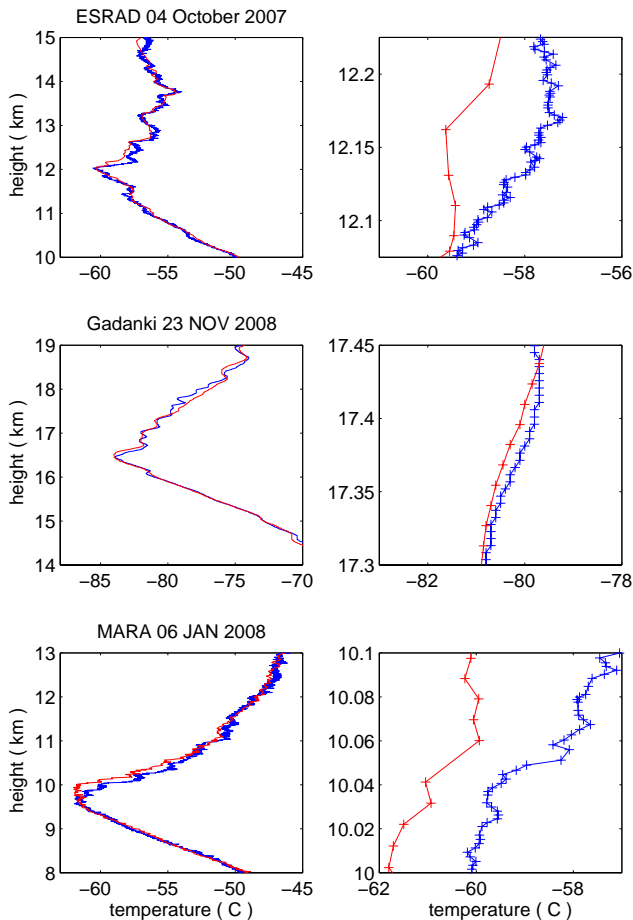
Fig. 7. Examples of temperature profiles close to the tropopause at each site, showing fine structure. Blue lines were measured on ascent, red lines on descent. Circles on the right-hand panels show the heights of each measurement taken by the sondes.

described by $F^2(\lambda)$ is close to the same, possibly exactly the same, at all three locations in the present study, and at Poker Flat in Alaska.

For UTLS results interpreted as volume scatter (Fig. 6), the best-fit lines are parallel but offset. The offsets correspond to the relative A_{eff} of the respective antenna arrays, which is the result to be expected according to Eq. (7), given that there are no significant offsets in Fig. 5. It is in principle possible that the volume-scatter model as described by Eq. (2) might be appropriate, but the aspect sensitivity measurements in Fig. 4 suggest otherwise, and it would then be a remarkable coincidence that the average values of L_o at the three sites differed by just the same amounts as A_{eff}. A more reasonable conclusion is that this confirms what is expected – i.e. that scatter from the UTLS is highly aspect sensitive and better matched by a Fresnel scattering model than by volume scatter.

For the lower troposphere, the spread of observations about the fitted lines is very large. However, even at these heights, the observations support the interpretation that the Fresnel scatter model provides a better fit than volume scatter, (i.e. the offsets between the fitted lines for the different radars are less in the Fresnel scatter interpretation). If the scatter in the lower troposphere was predominantly volume scatter, and if average values of L_o were the same at the three radar locations, we would rather expect the offsets to be very small for the volume reflectivity interpretation. The uncertainties in determining the constant of proportionality between $|\rho|^2 \Delta r$ or η and M^2 are quite large. In the volume scatter interpretation (Fig. 6) the fits (together with calibration uncertainties) give $\eta = 1 - 6 \times M^2$ for ESRAD, $3 - 36 \times M^2$ for Gadanki, and $0.1–0.2 \times M^2$ for MARA. Despite the large uncertainties, there are significant differences between the value for MARA and for the other two radars. In the Fresnel scatter interpretation (Fig. 5), the results are $\rho|^2/\Delta r = 1 - 8 \times 10^{-3} \times M^2$ for ESRAD, $2 - 30 \times 10^{-3} \times M^2$ for Gadanki, and $0.5 - 2 \times 10^{-3} \times M^2$ for MARA, i.e. there is no significant difference between the sites. This suggests that aspect sensitive scatter dominates the average power for radar returns at vertical incidence even in the lower troposphere, at least in the examples used in the present study, although it is clear from the aspect-sensitivity estimates in Fig. 4 that isotropic scatter also occurs. This is in line with the observations in Fig. 4, showing several instances of low values of ϕ_s in the lower troposphere, and with results of Ghosh et al. (2004) who used beam-swinging experiments to examine aspect sensitivity with the Gadanki radar and found evidence for high aspect sensitivity at times in the lower troposphere when the static stabilty was high. Even if volume scatter also does occur, it seems that the aspect sensitive echoes dominate the scattered power, at least in an average sense.

Finally, we note that the same average relation $|\rho|^2/\Delta r = 2 \times 10^{-3} \times M^2$ is consistent with the measurements, throughout the height range represented by our measurements, and for all three sites.

6   Fine structure comparison

The theory of Fresnel scatter is based on the concept of quasi-specular reflection by horizontal boundaries each representing a finite temperature step, distributed in height in some way characterised by $F(\lambda)$ (on average over the probed volume). To make a quantitative comparison between our results and the theory, we first consider scatter from single boundaries. Figure 7 shows examples, one from each site, of the fine structure of the temperature profiles at the best resolution available. At ESRAD and MARA, the temperature is sampled at about 2.5 m vertical resolution on ascent (2 samples/s at an ascent rate of 5 m/s). This corresponds closely to the vertical fluctuation scale to which 50 MHz radars are sensitive (3 m). At Gadanki, the resolution is about 5 m on ascent. The vertical resolution on descent is less good, but there is
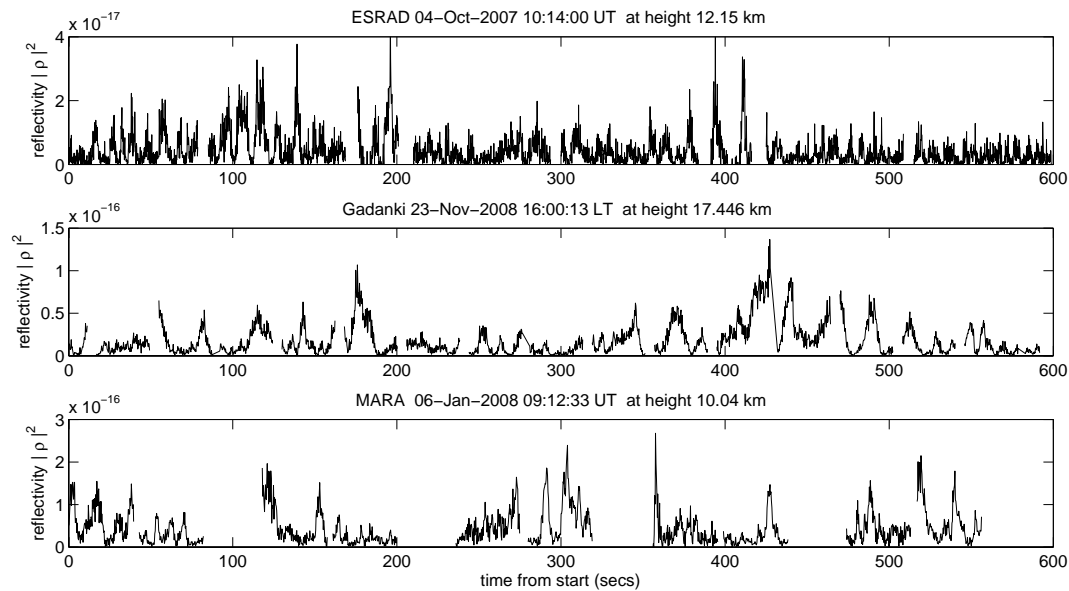
Fig. 8. Time sereis of reflectivity measurements from tropopause heights for each radar at 200–300 ms time resolution. A representative time period of 600 s is shown for each radar. Note that Fresnel reflectivity $|\rho|^2$ rather than Fresnel scatter $|\rho|^2/\Delta r$ is plotted here for ease of comparison with the theoretical value for single-boundary reflectivity.

still enough information to see that the temperature gradient above the tropopause is distinctly step-like. On vertical scales of 100 m or more (left hand panels of Fig. 7), steps of order 1 °C are seen, at roughly the same height on both ascent and descent. So these layer boundaries extend over 10s of km. On the 2–5 m vertical scale (right hand panels of Fig. 7), the sondes at ESRAD and at MARA show steps of between 0.1 and 0.5 °C between successive measurements, only 2.5 m apart. The large step at 10.05 km height on 6 January 2008 can be seen on both ascent and descent showing that it is likely real, and horizontally extended. The sonde at Gadanki shows much smoother profiles on this vertical scale but this may be due to limited sonde response time, as a different kind of sonde is used there.

The sharp steps in temperature seen by the high-resolution sondes at MARA and ESRAD are consistent with the evidence reported by Dalaudier et al. (1994) for "sheets" in the temperature field (in the mid-latitude atmosphere). Using balloon-borne temperature sensors with very fast response time, those authors were able to show that sheets typically 3–20 m thick, with temperature steps 0.2–0.8 K, gradients 0.3–1 K/km and horizontal extent in excess of 100 m, were common in regions of high static stability.

Following Gage (1990), a single boundary, extending horizontally by at least the radius of the first Fresnel zone (about 200 m in these cases), at about the height of the tropopause, with a temperature step of 0.1 °C should result in a Fresnel reflectivity $|\rho|^2 = 3 \times 10^{-16}$. A temperature step of 0.5 °C would give 25 times more. Interpreted as Fresnel scatter, using a probing resolution of 600 m, these correspond to $|\rho|^2/\Delta r = 5 - 125 \times 10^{-19}$ m^{-1}, which is much higher than

even the strongest echoes in our data set (see Fig. 5). To try to understand this further, we next compare with radar measurements at high time resolution, rather than the 1 h averages which we have considered up to now.

Figure 8 shows typical examples of measurements from each radar, now processed to show Fresnel reflectivity ($|\rho|^2$) at a time resolution of about 200 ms. The heights selected match the high-resolution temperature profiles in Fig. 7. It is clear that the reflectivity varies substantially on scales of a few seconds. Here we can see that values of $|\rho|^2$ approaching 3×10^{-16} are indeed observed, as could be expected from temperature steps of 0.1 °C. The much lower values in our 1 h averages result from the very short duration of these "flashes" of specular reflection.

It is clear from measurements using the interferometric capabilities of ESRAD and MARA that the "flashes" move horizontally with the background wind. Their motion is used routinely to determine wind speed using the spaced antenna technique and the resultant winds agree well with those measured by radiosondes (see e.g. Kirkwood et al., 2010; Valkonen et al., 2010). A possible explanation is that they are due to undulations in the reflecting surfaces, which sometimes are flat or concave, allowing constructive interference of the wave front returned to the radar, but mostly are convex or irregular, substantially reducing the effectiveness of the reflection. This concept is also supported by the observations of spatial variability of the temperature sheets reported by Dalaudier et al. (1994). It was found that the sheets are not flat, with distortions in the vertical direction by up to 10 m on horizontal scales of a few 10s of meters.

This temporal variability of the radar echoes implies that some modification of the Fresnel scattering model is needed. The fine structure term $F(\lambda)$ should be a time average as well as (or possibly instead of) a spatial average. It is interesting to note that the temporal variability appears similar at all three sites, consistent with the similar average values of $F(\lambda)$ for the three sites. There is however, no obvious reason why this should be the case, nor any reason why it should be similar at all heights.

It is interesting to consider how the intermittency of the signal illustrated in Fig. 8 will affect signal spectral widths, which are often interpreted as a measure of turbulent motion in the scattering volume. Spectral widths are found by Fourier transform applied to short time series, typically a few seconds, or a few 10s of seconds, long. They may often include only a single peak in the signal. The spectral width will depend primarily on the time duration of the peak and will have very little to do with turbulent motion. In some cases, the signal peaks appear quasi-periodic (e.g. in the first 200 s of the time series shown for ESRAD in Fig. 8). This may be due wave-like undulations in a scattering surface. Again, spectral analysis will be dominated by such wave effects and will not be related to turbulence. In general, it seems that spectral analysis of such strongly intermittent signals is not a useful technique for studying turbulence.

7 Conclusions

Three 50 MHz radars, ESRAD in Arctic Sweden, the Gadanki MST radar in tropical India, and MARA in Antarctica have been calibrated in the same way. Regular calibration is achieved using the daily variation of galactic radio noise, with the accuracy of this method confirmed by engineering calibration methods.

Calibrated radar measurements and radiosonde profiles from the troposphere and lower stratosphere have been used to explore quantitatively the relationship between the vertical gradient of generalized refractive index, M, and two models of radar reflectivity, Fresnel scatter, $|\rho|^2/\Delta r$ and volume scatter, η. The Fresnel scatter model leads to the same constant of proportionality between $|\rho|^2/\Delta r$ and M^2 at all three sites, for all upper tropospheric and lower stratospheric heights, for radar measurements averaged over 30 min–1 h. For the lower troposphere the uncertainty in determining the constant of proportionality is high, but the same value as found for the UTLS is within the bounds of the uncertainty, at all three sites. There is no obvious explanation why this should be so as the proportionality should depend on the details of the fine-structure of the refractive index profile at 3 m vertical scale. This might rather be expected to vary both with height and location.

The volume scatter model leads to systematic offsets between the three sites in the constant of proportionality between η and M^2. The simplest explanation for this is that as-pect sensitive scatter (Fresnel scatter) dominates the average backscattered power for vertically directed radar beams as used in this study, although aspect-sensitivity measurements show that volume (isotropic) scatter also occurs.

High-resolution radiosonde profiles indicate the presence of discrete temperature steps of order 0.1–0.5 °C at close to 3 m vertical scale. Average Fresnel reflectivities ($|\rho|^2$) are much lower than would be expected to result from specular (Fresnel) reflection from such boundaries. Time series of reflectivity with 200 ms time resolution, however, show that "flashes" of reflectivity approaching those expected from such boundaries occur sporadically. We suggest that this is caused by undulations on the reflecting surfaces, as they are carried across the radar by the wind. At high time resolution it is clear that reflectivity is highly variable, so that the model of Fresnel scatter needs to be modified to include the concept of time averaged fine structure as well as (or instead of) spatial fine structure.

Time-averaged Fresnel reflectivities should then depend on the spatial properties of the undulations in the reflecting layers. There is, however, no obvious reason why these should conspire to create the same constant of proportionality between $|\rho|^2/\Delta r$ and M^2 at all tropospheric heights and in both polar regions plus the tropics. It seems our understanding of Fresnel scatter for 50 MHz radar is still far from complete.

References

Alvarez, H., Aparici, J., May, J., and Olmos, F.: A 45-MHz continuum survey of the southern hemisphere, Astron. Astrophys. Suppl. Ser., 124, 315–328, 1997.

Belova, E., Kirkwood, S., Rao, T. N., Kumar, S. S., and Sergienko, T.: Mesospheric winter echoes from polar and low latitudes: comparison of spectral characteristics and strength, Ann. Geophys., in review, 2010.

Campistron, B., Despaux, G., Lothon, M., Klaus, V., Pointin, Y., and Mauprivez, M.: A partial 45 MHz sky temperature map obtained from the observations of five ST radars, Ann. Geophys., 19, 863–871, doi:10.5194/angeo-19-863-2001, 2001.

Chilson, P., Kirkwood, S., and Nilsson, A.: The Esrange MST radar: A brief introduction and procedure for range validation using balloons, Radio Sci., 34, 427–436, 1999.

Dalaudier, F., Sidi, C., Crochet, M., and Vernin, J.: Direct evidence of 'sheets' in the atmospheric temperature field., J. Atmos. Sci., 51, 237–248, doi:10.1175/1520-0469(1994)051, 1994.

de Oliveira-Costa, A., Tegmark, M., Gaensler, B. M., Jonas, J., Landecker, T. L., and Reich, P.: A model of diffuse Galactic radio emission from 10 MHz to 100 GHz, Mon. Not. Roy, Astron. Soc., 388, 247–260, doi:10.1111/j.1365-2966.2008.13376.x, 2008.

Doviak, R. J. and Zrnic, D. S.: Reflection and scatter formula for anisotropically turbulent air, Radio Sci., 19, 325–336, doi:10.1029/RS019i001p00325, 1984.

Ellington, S.: Antennas for the next generation of low-frequency radar telescopes, IEEE Transactions on Antennas and Propagation, 53, 2480–2489, 2005.

Gage, K.: Radar observations of the free atmosphere: structure and dynamics, in: Radar in Meteorology, edited by: Atlas, D., chap. 28a, pp. 534–565, American Meteorological Society, Boston., 1990.

Gage, K. S. and Green, J. L.: Evidence for specular reflection from monostatic VHF radar observations of the stratosphere, Radio Sci., 13, 991–1001, doi:10.1029/RS013i006p00991, 1978.

Gage, K. S., Balsley, B. B., and Green, J. L.: Fresnel scattering model for the specular echoes observed by VHF radar, Radio Sci., 16, 1447–1453, doi:10.1029/RS016i006p01447, 1981.

Gage, K. S., Ecklund, W. L., and Balsley, B. B.: A modified Fresnel scattering model for the parameterization of Fresnel returns, Radio Sci., 20, 1493–1501, doi:10.1029/RS020i006p01493, 1985.

Ghosh, A. K., Das, S. S., Patra, A. K., Rao, D. N., and Jain, A. R.: Aspect sensitivity in the VHF radar backscatters studied using simultaneous observations of Gadanki MST radar and GPS sonde, Ann. Geophys., 22, 4013–4023, doi:10.5194/angeo-22-4013-2004, 2004.

Hocking, W. K.: Measurement of turbulent energy dissipation rates in the middle atmosphere by radar techniques: A review, Radio Sci., 20, 1403–1422, doi:10.1029/RS020i006p01403, 1985.

Hocking, W. K.: VHF tropospheric scatterer anisotropy at Resolute Bay and its implications for tropospheric radar-derived wind accuracies, Radio Sci., 36, 1777–1794, doi:10.1029/2000RS001002, 2001.

Hocking, W. K., Ruester, R., and Czechowsky, P.: Absolute reflectivities and aspect sensitivities of VHF radio wave scatterers measured with the SOUSY radar, J. Atmos. Terr. Phys., 48, 131–144, 1986.

Holdsworth, D. A.: Influence of instrumental effects upon the full correlation analysis, Radio Sci., 34, 643–656, doi:10.1029/1999RS900001, 1999.

Holdsworth, D. A. and Reid, I. M.: A simple model of atmospheric radar backscatter: Description and application to the full correlation analysis of spaced antenna data, Radio Sci., 30, 1263–1280, doi:10.1029/95RS00645, 1995.

Hooper, D. A., Arvelius, J., and Stebel, K.: Retrieval of atmospheric static stability from MST radar return signal power, Ann. Geophys., 22, 3781–3788, doi:10.5194/angeo-22-3781-2004, 2004.

Kirkwood, S., Mihalikova, M., Rao, T. N., and Satheesan, K.: Turbulence associated with mountain waves over Northern Scandinavia – a case study using the ESRAD VHF radar and the WRF mesoscale model, Atmos. Chem. Phys., 10, 3583–3599, doi:10.5194/acp-10-3583-2010, 2010.

Kirkwood, S., Wolf, I., Nilsson, H., Dalin, P., Mikhaylova, D., and Belova, E.: Polar mesosphere summer echoes at Wasa, Antarctica (73 degrees S): First observations and comparison with 68 degrees N, Geophys. Res. Lett., 34, L15803, doi:10.1029/2007GL030516, 2007.

Kirkwood, S., Nilsson, H., Morris, R. J., Klekociuk, A. R., Holdsworth, D. A., and Mitchell, N. J.: A new height for the summer mesopause: Antarctica, December 2007, Geophys. Res. Lett., 35, L23810, doi:10.1029/2008GL035915, 2008.

Luce, H., Hassenpflug, G., Yamamoto, M., and Fukao, S.: Comparisons of refractive index gradient and stability profiles measured by balloons and the MU radar at a high vertical resolution in the lower stratosphere, Ann. Geophys., 25, 47–57, doi:10.5194/angeo-25-47-2007, 2007.

Maeda, K., Alvarez, H., Aparici, J., May, J., and Reich, P.: A 45-MHz continuum survey of the northern hemisphere., Astron. Astrophys. Suppl. Ser., 140, 145–154, 1999.

Rao, P. B., Jain, A. R., Kishore, P., Balamuralidhar, P., Damle, S. H., and Viswanathan, G.: Indian MST radar 1. System description and sample vector wind measurements in ST mode, Radio Sci., 30, 1125–1138, doi:10.1029/95RS00787, 1995.

Rao, T. N., Arvelius, J., and Kirkwood, S.: Climatology of tropopause folds over a European Arctic station (Esrange), J. Geophys. Res., 113, D00B03, doi:10.1029/2007JD009638, 2008.

Tsuda, T., May, P. T., Sato, T., Kato, S., and Fukao, S.: Simultaneous observations of reflection echoes and refractive index gradient in the troposphere and lower stratosphere, Radio Sci., 23, 655–665, doi:10.1029/RS023i004p00655, 1988.

Valkonen, T., Vihma, T., Kirkwood, S., and Johansson, M.: Fine-scale model simulation of gravity waves generated by Basen nunatak in Antarctica, Tellus, 62A, 319–332, doi:10.1111/j.1600–0870.2010.00443.x, 2010.